Published in final edited form as:

Al-Naji, M., Puértola, B., Kumru, B., Cruz, D., Bäumel, M., Schmidt, B. V. K. J., et al. (2019). Sustainable continuous flow valorization of γ-valerolactone with trioxane to α-methylene-γ-valerolactone over basic beta zeolite. ChemSusChem, 12(12), 2628-2636. doi:10.1002/cssc.201900418.

Sustainable continuous flow valorization of γ-valerolactone with trioxane to α-methylene-γ-valerolactone over basic beta zeolite

Majd Al-Naji, Begoña Puértolas, Baris Kumru, Daniel Cruz, Marius Bäumel, Bernhard V.K.J. Schmidt, Nadezda V. Tarakina, and Javier Pérez-Ramírez

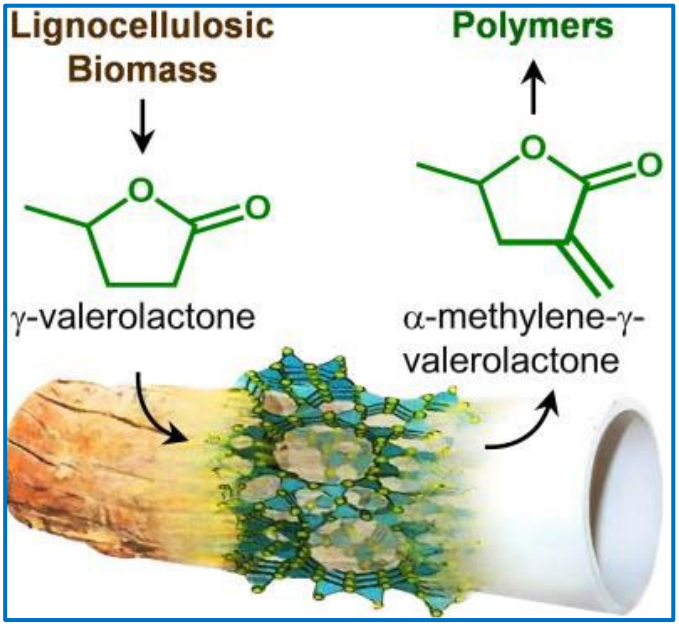

Sustainable tandem flow process: MeGVL was synthesized from lignocellulosic biomass-derived GVL in the presence of trioxane using tailored Cs-loaded hierarchical beta zeolite catalysts. The obtained MeGVL was subjected to visible-light-induced polymerization reaction, reaching a final material with similar properties to poly(methyl) methacrylate.

Cover

https://doi.org/10.1002/cssc.201901510

M. Al-Naji et al.

Sustainable Continuous Flow Valorization of γ-Valerolactone with Trioxane to α-Methylene-γ-Valerolactone over Basic Beta Zeolites

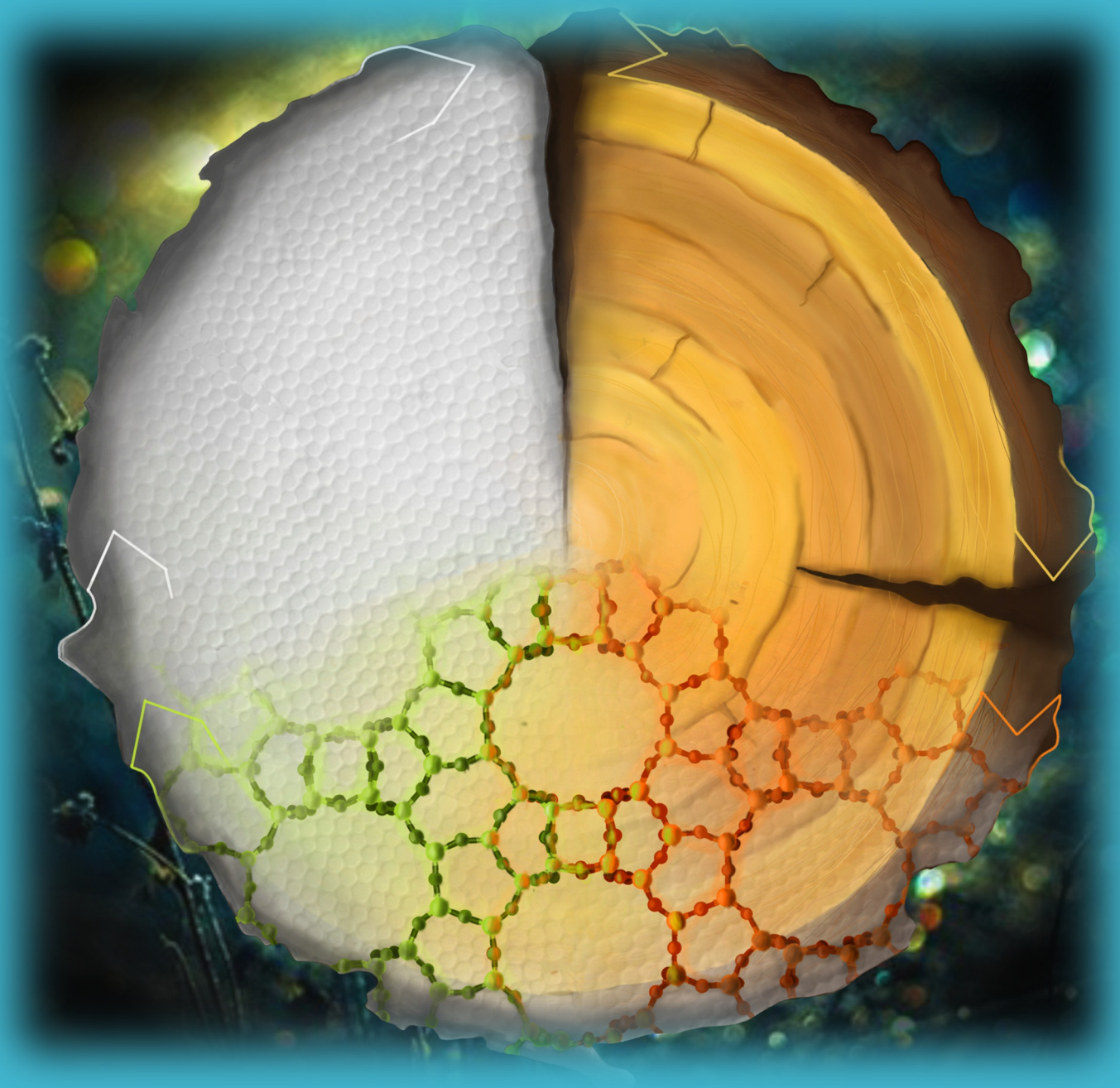

Sustainable Continuous Flow Valorization of γ-Valerolactone with Trioxane to α-Methylene- γ-Valerolactone over Basic Beta Zeolites

Majd Al-Naji,*[a,†] Begoña Puértolas,[b,†] Baris Kumru,[a] Daniel Cruz,[a] Marius Bäumel,[a] Bernhard V.K.J. Schmidt,[a] Nadezda V. Tarakina,[a] and Javier Pérez-Ramírez[b]

Abstract: The necessity of more sustainable products and processes has led to the use of new methodologies which result in a low carbon footprint. Here, we demonstrated an efficient tandem process for the liquid-phase catalytic upgrading of lignocellulosic biomass-derived γ-valerolactone (GVL) with trioxane (Tx) to α-methylene-γ-valerolactone (MeGVL) in flow using Cs-loaded hierarchical beta zeolites. The introduction of mesopores along with the presence of basic sites of mild strength led to 20-times higher MeGVL productivity compared to the bulk beta zeolite reaching 0.325 mmol min^{-1} g_{cat}^{-1} for the best-performing catalyst, the highest value reported so far. This catalyst proved stable upon reuse in consecutive cycles, which was ascribed to the partial depletion of the basic sites. The obtained MeGVL was subjected to visible-light-induced polymerization resulting into a final material with similar properties to the widely used poly(methyl) methacrylate.

Introduction

The necessity for the green manufacture of fine chemicals and polymers motivate the search of novel processes based on renewable and sustainable resources.[1-7] In particular, lignocellulosic biomass consisting of cellulose, hemicellulose, and lignin fractions, represents one of the most abundant and economical starting materials.[1] The prospective of lignocellulosic biomass as a substrate for the efficient production of building blocks such as levulinic acid, GVL, 5-hydroxymethylfuran (HMF) and dimethyl furan (DMF) has been already demonstrated at the lab-scale.[4, 8-13] Among them, GVL produced *via* the hydrodeoxygenation of lignocellulosic biomass, exhibits excellent solvent properties and is one of the main precursors in the synthesis of high-value fine chemicals and polymers, such as pentenoic acid, valeric acid and MeGVL.[1, 4, 14, 15] In this regard, MeGVL is a type of methacrylic monomer with the potential to substitute the fossil-based methyl methacrylate (MMA), a monomer produced on a large scale for the production of poly(methyl methacrylate), the latter having numerous applications in the automotive, electronics, and medical sectors.[1, 2, 16] The non-catalytic synthesis of MeGVL using GVL as precursor was patented in 1953 using GVL and ethyl formate in ethanol in the presence of granulated sodium sand.[17] In the absence of catalyst, a two-step process using ethyl formate and paraformaldehyde and tetrahydrofuran or dimethylsulfoxide as solvents was also reported.[18] Even though the yield of MeGVL obtained was *ca.* 90%, the use of non-environmentally-friendly organic solvents along with the moderate kinetics make their practical implementation unfeasible. More recently, the catalytic synthesis of MeGVL was approached *via* the base-catalyzed α-methylation reaction in batch using either aqueous formaldehyde (FA) solution, *i.e.*, formalin, or paraformaldehyde as FA source (**Scheme 1**). The use of a base enables the nucleophilic attack of FA on the α-position of GVL, a step that is essential for the subsequent conversion into MeGVL. The MeGVL yield was limited to 36% using an homogeneous base, *i.e.*, K_2CO_3 and $CsCO_3$, in the presence of paraformaldehyde and 2-methyltetrahydrofuran (MeTHF) or supercritical CO_2 as solvents.[19, 20] A step forward towards the continuous operation using different rare earth metals supported on silica was also reported.[21] Although GVL was converted to a large extent, *i.e.*, 60%, no information regarding the selectivity towards the desired MeGVL is available.

In this work, we investigated the development of a sustainable tandem process in flow for MeGVL synthesis from lignocellulosic biomass-derived GVL in the presence of Tx using tailored Cs-loaded hierarchical beta zeolite catalysts (**Scheme 1**). The use of Tx instead of FA, the latter generally available in aqueous solutions, is believed to increase the yield of MeGVL as the presence of water inhibits the α-methylation reaction. The decomposition of Tx in the temperature range 483-503 K leads to the formation of 3 molecules of FA that are essential to initiate the desired transformation.[22-24] The comparative impact of the porous, acidic, and basic properties of the zeolites upon Cs loading on the yield of MeGVL is quantified, providing insights into the enhanced selectivity observed over the hierarchical zeolites. The synthesized MeGVL over the best-performing material was subjected to visible-light induced polymerization to produce poly(MeGVL) using graphitic-carbon nitride (*g*-CN) as catalyst.[25-28]

[a] Dr. M. Al-Naji, B. Kumru, D. Cruz, M. Bäumel, Dr. B.V.K.J. Schmidt, Dr. N.V. Tarakina
Department of Colloid Chemistry
Max Planck Institute of Colloids and Interfaces
Am Mühlenberg 1, 14476 Potsdam (Germany)
E-mail: majd.al-naji@mpikg.mpg.de

[b] Dr. B. Puértolas, Prof. J. Pérez-Ramírez
Department of Chemistry and Applied Biosciences, ETH Zurich
Institute for Chemical and Bioengineering
Vladimir-Prelog-Weg 1, 8093 Zurich (Switzerland)

[†] These authors have contributed equally

Supporting information for this article is given via a link at the end of the document.

Results and Discussion

GVL valorization over zeolites with different framework topologies

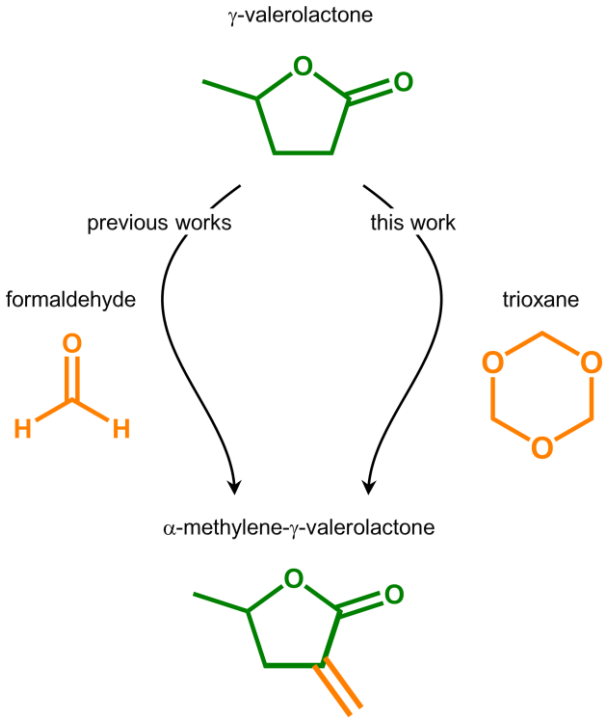

Scheme 1. Traditional pathway for the synthesis of MeGVL from GVL in the presence of FA from formalin or paraformaldehyde (left). The new tandem route demonstrated in this work that uses trioxane as formaldehyde source (right).

To date, the availability of studies tackling the valorization of GVL into MeGVL over heterogeneous catalysts is scarce. Accordingly, we firstly assessed the performance of commercial zeolites in acidic form with different framework topology and Si/Al ratio in the α-methylation of GVL at 568 K in flow (**Figure 1a** and **Figure S1**). After 1 h on stream, the conversion of GVL obtained over ZSM-5 (Si/Al = 140) and mordenite (Si/Al = 10) zeolites was lower than that over the beta (Si/Al = 150) zeolite. Increasing the Si/Al ratio to 220 led to a further increase of the GVL conversion, which could be associated to the presence of stronger acid sites in this sample in comparison to beta-150. It is worth noticing that trioxane was fully converted in all cases. However, the yield of MeGVL was very low for all the materials, and the major formation of ring-opening compounds such as 4-pentonoic acid and butene as side products was observed (**Figure S2**). The latter was only noticeable in the case of the beta zeolites as the lower GVL conversion obtained when ZSM-5 and mordenite zeolites were used impeded the quantification of the products formed. The selectivity towards the desired MeGVL product increases upon the introduction of Cs (**Figure 1b**, **Figure S2**, and **Table S1**). Comparison between the performance of the Cs-containing sample and the parent material revealed the key role of Cs in catalyzing the α-methylation of GVL to MeGVL. The formation rate of MeGVL slightly decreases upon increasing the Si/Al ratio of the framework for the Cs-loaded zeolites, *i.e.*, 0.133 and 0.126 $mmol_{MeGVL}$ min^{-1} g_{cat}^{-1} for the 5Cs/beta-150 and 5Cs/beta-220 materials, respectively. The rest of the products formed account for 4-pentenoic acid and methyl 4-pentenoate as the main compounds, the latter likely formed upon the reaction between 4-pentenoic acid and the methanol formed from the decomposition of FA at high temperatures (**Figure S1**). In contrast to the commercial materials, the formation of butane, 2-butanol, 2-pentene, and pentanal are suppressed, which suggests the occurrence of a different reaction mechanism in the presence of Cs. In view of the slightly higher productivity of MeGVL, beta zeolite with Si/Al 150 and cesium loading of 5 wt.% was selected for further investigation.

Post-synthetic modification of beta zeolites by alkaline treatment and cesium loading

The parent beta (Si/Al = 150) zeolite was subjected to an alkaline treatment, attaining, after ion exchange to its acidic form, a hierarchical analog coded H-beta-150. The composition and textural properties are summarized in **Table 1**. As expected, the

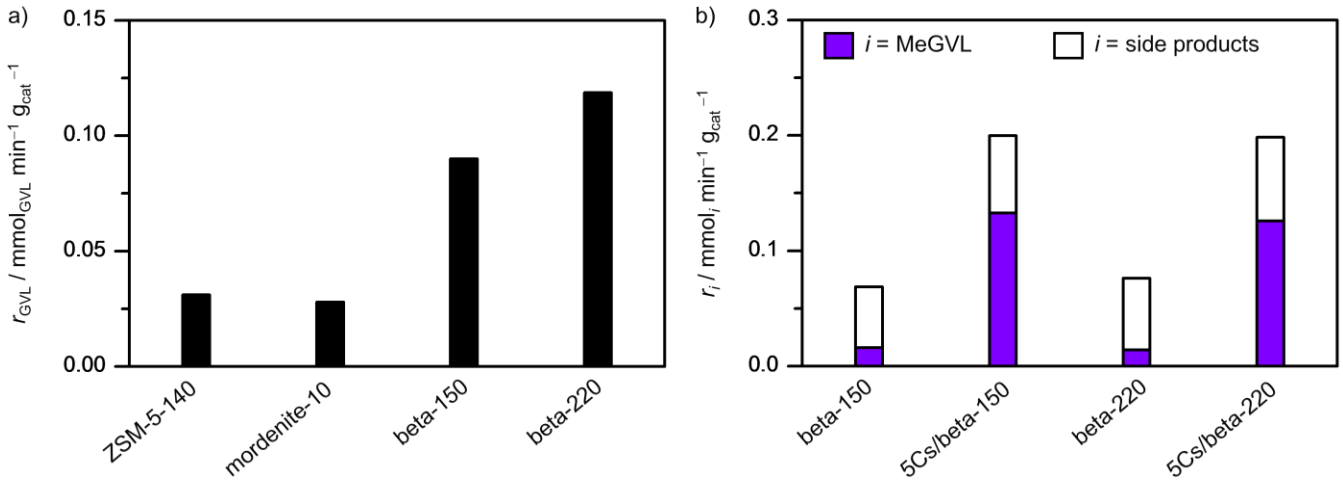

Figure 1. a) Rate of conversion of GVL and b) rate of formation of MeGVL and side products over zeolites with different framework topologies and Si/Al ratios prior to and after cesium loading. Reaction conditions: m_{cat} = 3 g, m_{GVL} = 5.1 g, m_{Tx} = 10.1 g, V_{MeTHF} = 500 cm^3, $Q_{reactant}$ = 0.3 cm^3 min^{-1}, τ = 13.8 min, and $V_{reactor}$ = 4.15 cm^3.

Table 1. Characterization data of the catalysts.

Catalyst	Si/Al	Cs loading[a] (wt.%)	V_{pore}[b] ($cm^3\ g^{-1}$)	V_{micro}[c] ($cm^3\ g^{-1}$)	S_{meso}[c] ($m^2\ g^{-1}$)	S_{BET}[d] ($m^2\ g^{-1}$)	Cryst. (%)
beta-150	150	-	0.39	0.23	150	582	100
H-beta-150	115	-	0.74	0.17	351	677	74
5Cs/beta-150	146	5	0.30	0.13	132	388	45
5Cs/H-beta-150	110	4.9	0.59	0.12	253	491	44
5Cs/H-beta-150 used 1st cycle	111	4.9	0.45	0.12	151	383	19
5Cs/H-beta-150 reg. after 3rd cycle	116	4.8	0.68	0.16	266	565	38
10Cs/H-beta-150	109	9.6	0.47	0.11	192	395	45
23Cs/H-beta-150	114	22	0.37	0.09	152	318	2
5Cs/SiO_2	-	4.7	0.75	-	-	550	-

[a] ICP-OES. [b] Volume adsorbed at $p/p_0 = 0.99$. [c] *t*-plot method. [d] BET method.

desilication led to the development of additional mesoporous area, which was accompanied by a drop in crystallinity and microporous volume. In addition, the Si/Al ratio decreased with the consequent increase of the amount of charge-compensating H^+ cations. The incorporation of different amounts of Cs, *i.e.*, 5, 10, and 23 wt.% by dry impregnation led to a further decrease of the textural properties and crystallinity as the amount of Cs increases (**Table 1** and **Table S1**). These samples are called *x*Cs/H-beta-150, where *x* refers to the Cs loading.

The basicity of the hierarchical beta zeolites with different Cs loadings was assessed by CO_2-TPD (**Figure 2a**). The parent and the hierarchical zeolites produced no significant desorption, confirming their negligible basicity. In contrast, two major peaks centered at 410 and 550 K became evident in the curves of the 5Cs/H-beta-150 zeolite, indicating the presence of basic sites with a moderate character. A fraction of Cs is expected to be present at ion exchange positions to balance the framework charge caused by the isomorphous substitution of silicon with aluminum atoms and possess very mild basicity.[29] Another part is believed to substitute the protons in the silanol groups present in defect-rich regions (*i.e.*, the external surface of the crystal or the mesopore walls), leading to stronger basic sites similar to those observed for high-silica faujasites.[30] Its occurrence was corroborated by XPS that revealed the presence of CsOH species on the catalyst surface (**Figure 2b**). Additionally, the occurrence of Cs_2O species was identified in the XPS spectrum, which could also contribute to the basicity. Regardless their speciation, Cs species are believed to be highly dispersed over the zeolite surface in line with STEM and XRD results that evidenced the absence of Cs-rich areas and Cs-containing nanoparticles (**Figure 3** and **Figure S3**), respectively. Acidity assessment by the infrared spectroscopy of pyridine adsorbed revealed the absence of acid sites in this sample, which is in line with the ion exchange of the protonic sites by cesium cations during the dry impregnation step. Increasing of the Cs loading led to the decrease of the density of mild basic sites and the formation of stronger basic sites (**Figure 2a**) in line with the appearance of a desorption peak centered at *ca.* 850 K. These sites could be the result of the agglomeration of different Cs-containing species as revealed by the micrographs of the sample prepared with the highest Cs loading (**Figure S4**). These species could contain

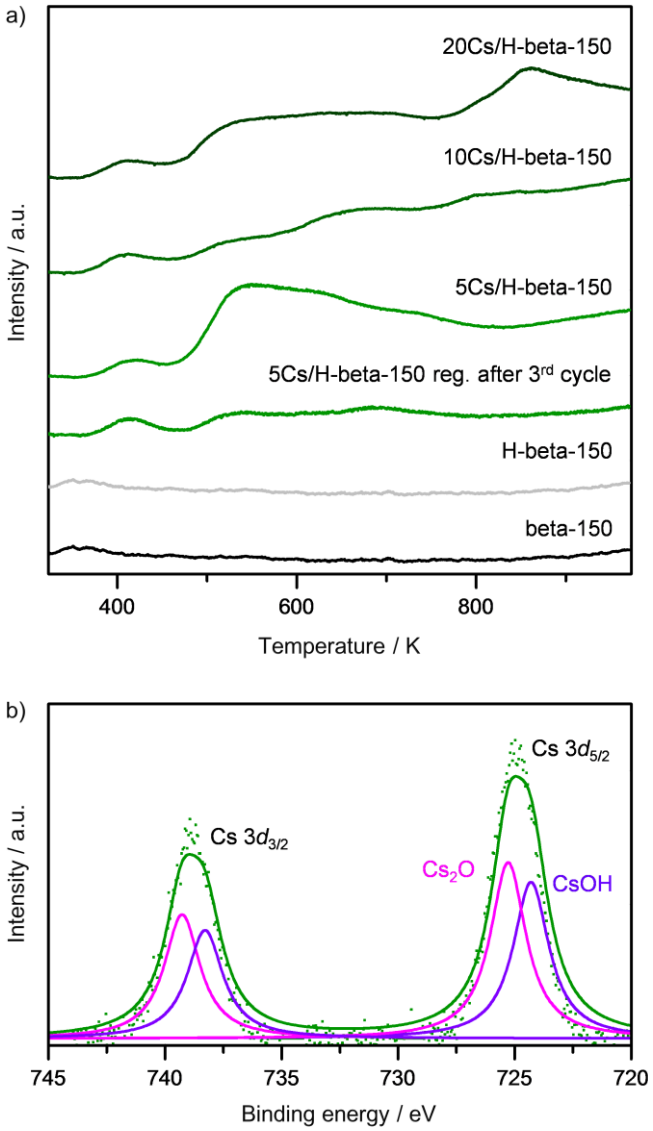

Figure 2. a) CO_2 desorption profiles of selected catalysts. b) Cs 3*d* core level spectra of 5Cs/H-beta-150 in fresh form.

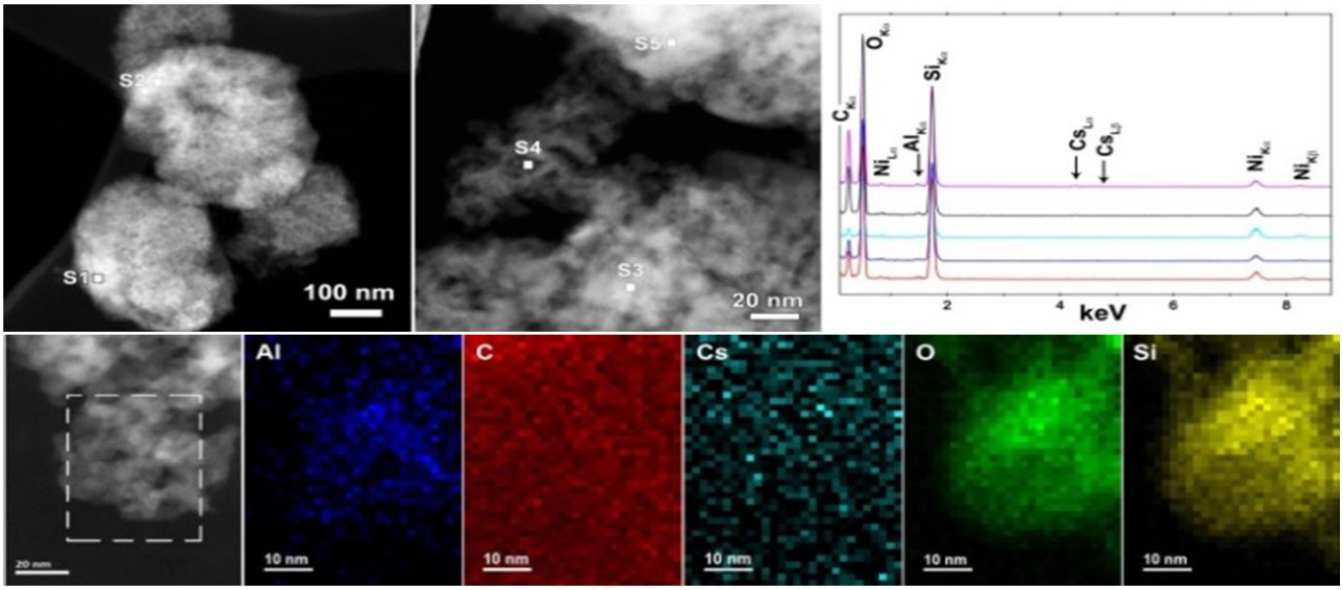

Figure 3. ADF-STEM images of 5Cs/H-beta-150 zeolite and EDX spectra at the location indicated in the micrograph.

CsO_2, Cs_2O_2, Cs_2O_3, Cs_2O_4, Cs_2O, Cs_7O, Cs metal, and any combination thereof that could be formed under a particular oxygen environment during calcination,[31] and whose identification is beyond the scope of the present study. In addition, a partial contribution from CsCl to the strong basicity cannot be discarded. XRD patters of the 23Cs/H-beta-150 catalyst (**Figure S3**) evidenced the characteristic reflections of this crystalline phase suggesting that it was not fully transformed into CsO_x species upon calcination.

Catalytic performance of Cs-loaded hierarchical zeolites

The mesoporous beta zeolites prepared through the post-synthetic treatments were tested as catalysts prior to and after Cs incorporation in the α-methylation of GVL under the same conditions as those applied to the screening of commercial zeolites presented above. Introduction of mesoporosity led to an increase of the conversion of GVL, which is accompanied by an increase in the formation of MeGVL (**Figure 4a**). Addition of 5 wt.% Cs to H-beta-150 led to a substantial increase in the amount of GVL converted along with the enhanced formation of MeGVL, *i.e.*, from 0.028 to 0.325 $mmol_{MeGVL}\ min^{-1}\ g_{cat}^{-1}$. Additionally, the rate of formation of undesired compounds decreased. In the case of the hierarchical H-beta-150 zeolite, the presence of 4-pentenoic acid, methyl-4-pentenoate, butene, 2-pentanol, 2-pentene is detected whereas only 4-pentenoic-acid and methyl-4-pentenoate are detected upon Cs incorporation (**Table S1, Figure S5**). In the case of the H-beta-150 material, the formation of undesired products could be attributed to the presence of acid sites of different strength that could catalyze the unselective conversion and/or the decomposition of GVL. However, the absence of acid sites in the 5Cs/H-beta-150 material led to a decrease formation of side products. Additionally, owing to the higher surface area, the hierarchical material could accommodate the carbon deposits associated to the occurrence of polymerization reactions more efficiently, in line with previous observations.[29] Therefore, the external surface area of the hierarchical sample decreased to a much lower extent than that of the bulk material (**Table 1 and Table S2**). It is worth mentioning that while the external surface area decreased upon reaction, the micropore volume remained unchanged, which might initially suggest that the investigated reaction does not require a microporous material. To discard this hypothesis, 5 wt.%Cs-loaded SiO_2 was synthesized using a SiO_2 support with the same average pore size as the H-beta-150 material. The results revealed that the 5Cs/SiO_2 material was less active than the 5Cs/H-beta-150 material (**Figure 4a**), thus highlighting the beneficial role of the microporous structure in the reaction.

The increase of the Cs loading over the H-beta-150 material lead to the increase of the amount of GVL converted at the expense of the decrease of the formation rate of MeGVL (**Figure 4b**). The latter is maximized over the sample with 5 wt.% Cs loading, which could be attributed to the presence of a higher density of mild basic sites along with the increased dispersion of the Cs species over the zeolite surface (**Figure 2a** and **Figure 3**). The presence of strong basic sites in the case of the samples with 10 and 23 wt.% led to lower amount of MeGVL formed with similar rate of formation of side products (**Figure 4b**). Comparison of the best-performing catalyst with the benchmark CsX zeolite led to 3-times higher formation rate of MeGVL. Additionally, CsX favored the conversion of GVL to a larger extent leading to the formation of an increase amount of side and polymerization products, mostly related to the occurrence of a higher density of basic sites with strong basicity over this sample.

Optimization of the reaction conditions

The reaction conditions were adjusted, in terms of temperature, Tx/GVL molar ratio, and residence time (τ), for the best catalyst, 5Cs/H-beta-150, to maximize the formation of MeGVL (**Figure 5**). With respect to temperature, two additional tests were conducted at 553 K and 583 K (**Figure 5a**). Under the milder conditions, a

drop in activity was observed. At the higher temperature, the amount of GVL converted was higher but the rate of formation of MeGVL substantially decreased. The dependence of the rate of GVL converted with the temperature is expected since the reaction kinetics increase with the temperature (**Figure S6**). Therefore, the use of 568 K is selected and the role of the Tx/GVL ratio was investigated under this condition (**Figure 5b**). In this case, two lower points were assessed, *i.e.*, 0.5 and 1, as a higher Tx/GVL was unfeasible due to the limited solubility of Tx in 2-methyltetrahydrofuran. In both cases, an activity depletion was determined, which was higher at the lower Tx/GVL. The better performance of the catalyst at Tx/GVL molar ratio of 2 suggests that the excess of FA generated from the decomposition of Tx is required for the efficient conversion of GVL. Applying 568 K and a Tx/GVL molar ratio of 2, the residence time was decreased to 5.9 and 8.3 min and increased to 41.5 min. As shown in **Figure 5c**, both the rate of conversion of GVL and the rate of formation of MeGVL reached a maximum for a residence time of 13.8 min. For shorter residence times, there is not enough contact between the substrates and the catalyst to ensure an efficient performance. In contrast, higher reaction times might lead to an increased

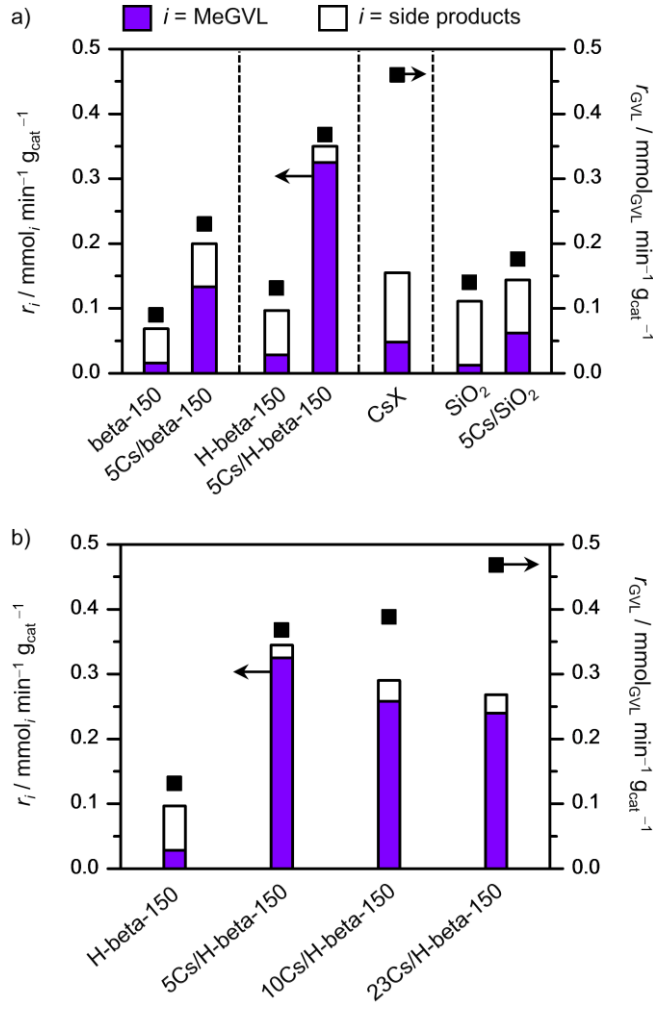

Figure 4. a) Rate of formation of MeGVL and side products and of conversion of GVL over bulk and hierarchical beta zeolites prior to and after cesium loading. The performance of CsX and Cs-loaded SiO_2 are included for comparative purposes. b) Rate of conversion of GVL and of formation of MeGVL and side products over hierarchical beta zeolites with different Cs loadings. Reaction conditions: m_{cat} = 3 g (bulk zeolite) and 2 g (hierarchical zeolite), m_{GVL} = 5.1 g, m_{Tx} = 10.1 g, V_{MeTHF} = 500 cm^3, $Q_{reactant}$ = 0.3 cm^3 min^{-1}, τ = 13.8 min, and $V_{reactor}$ = 4.15 cm^3.

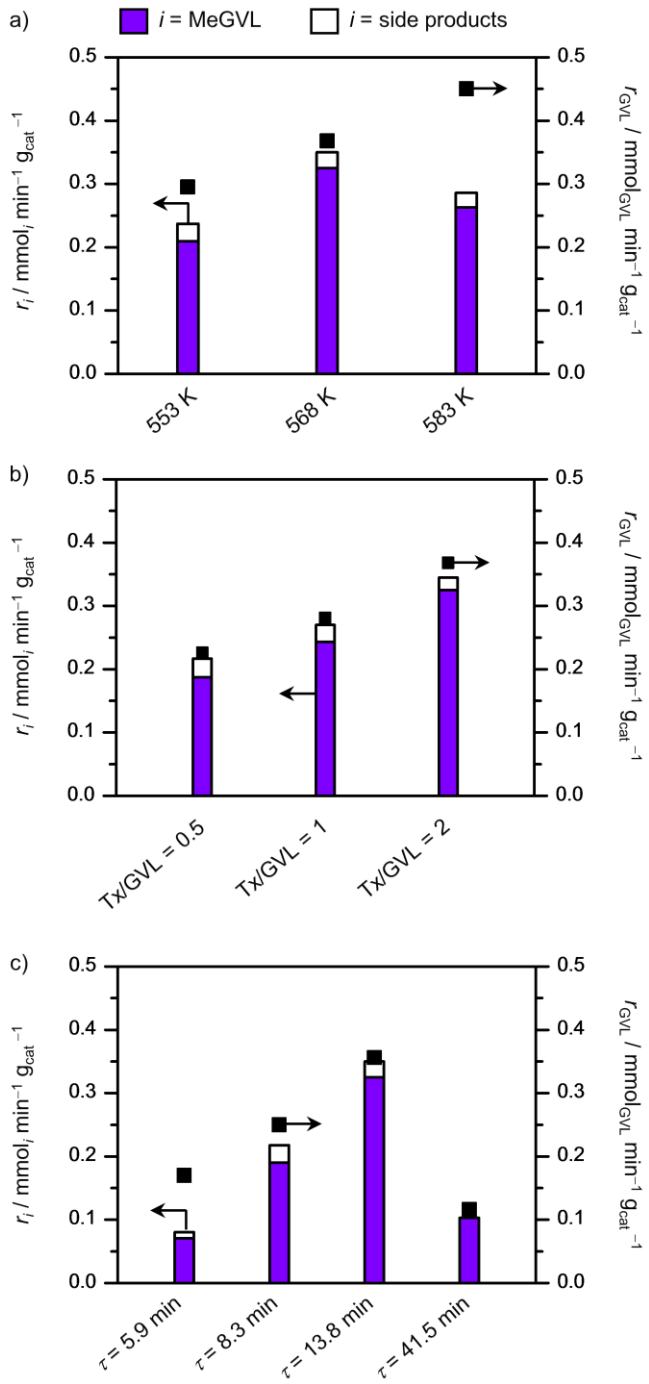

Figure 5. Impact of a) temperature, b) Tx/GVL molar ratio, and c) residence time on the rate of formation of MeGVL and side products and of conversion of GVL over 5Cs/H-beta-150 zeolite. Reaction conditions: m_{cat} = 2 g, m_{GVL} = 5.1 g, m_{Tx} = 10.1 g, V_{MeTHF} = 500 cm^3, $Q_{reactant}$ = 0.3 cm^3 min^{-1}, τ = 13.8 min and $V_{reactor}$ = 4.15 cm^3.

formation of carbon deposits on the catalyst surface owing to the higher contact time with the reactants.

Catalytic deactivation, regeneration, and reuse

The stability of the 5Cs/H-beta-150 zeolite was evaluated in a 6-h test (**Figure 6**). The catalyst performance was retained during the first 2 h, after which the zeolite started to deactivate and retained *ca.* 30% of the initial yield of MeGVL at the end of the run, in line with previous results by Lemonidou *et al*.[32] Coke formation and the strong adsorption of polymeric derivatives are believed to encompass the main routes for catalyst deactivation in the α-methylation of GVL. Characterization of the best-performing catalyst (5Cs/H-beta-150) by TGA confirmed the deposition of a conspicuous amount of coke, *i.e.*, 30 wt.% (**Figure S7**). This weight loss is divided in three different regions: region 1 (from 295 K to 500K) in which the weight loss of 4.9 wt.% corresponds to the desorption of physisorbed water, and regions 2 (from 575 K to 905 K) and 3 (from 910 K to 1150 K) in which the weight loss of 26 wt.% is assigned to the depletion of coke and large carbonaceous species on the catalyst. The porosity analysis uncovered the full preservation of the micropore volume and the halving of the mesopores (**Table 1**).

The implementation of reaction-regeneration cycles has been proposed as a strategy to extend the long-term use of the

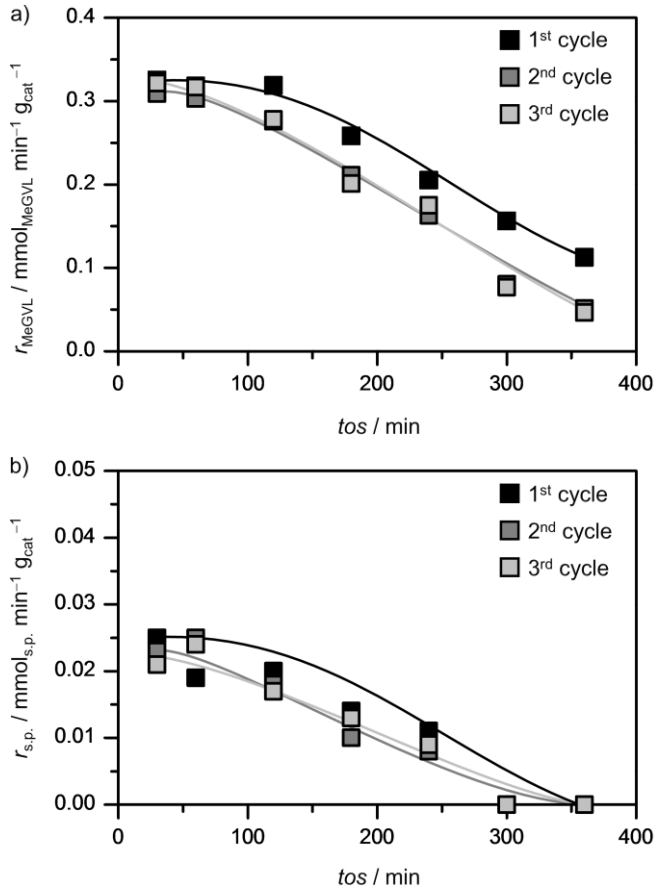

Figure 6. Rate of formation of a) MeGVL and of b) side products (s.p.) over 5Cs/H-beta-150 upon three subsequent catalytic cycles. Reaction conditions: m_{cat} = 2 g, m_{GVL} = 5.1 g, m_{Tx} = 10.1 g, V_{MeTHF} = 500 cm^3, $Q_{reactant}$ = 0.3 cm^3 min^{-1}, τ = 13.8 min, and $V_{reactor}$ = 4.15 cm^3.

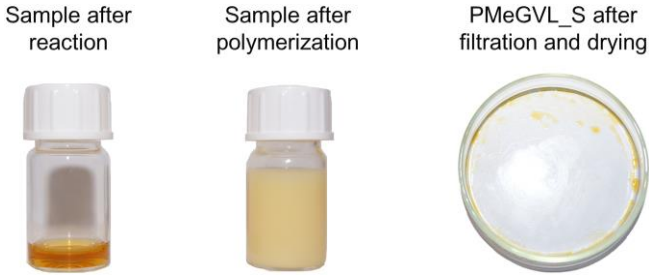

Figure 7. Withdrawn sample after reaction (left), sample after polymerization reaction (middle) using *g*-CN and the resulting polymer PMeGVL_S after filtration of *g*-CN and drying at 333 K (right).

catalysts (**Figure 6**). Herein, the activity of 5Cs/H-beta-150 zeolite was monitored over 2 consecutive runs between which the catalyst was thermally-treated in air to simulate a typical regeneration procedure. During the second test, the rate of formation of MeGVL slightly decreased compared to the first cycle, but both the MeGVL productivity and the formation of side prodcuts during the third cycle was fully retained (**Figure 6b**). Characterization of the regenerated sample after 3 cycles revealed that the textural properties and crystalline structure are mostly preserved (**Figure S3** and **Table 1**). CO_2-TPD analysis evidenced a decreased of the basic sites, especially of the milder type (**Figure 2a**). Since no Cs leaching was detected during the reaction (**Table 1**), Cs restructuring into different species upon regeneration is believed to be the origin of the changes in basicity determining the steady catalyst performance upon cycling.

Visible-light-induced MeGVL polymerization

As a proof of concept, MeGVL synthesized using 5Cs/H-beta-150 was subjected to visible-light-induced polymerization using graphitic carbon nitride (*g*-CN) as catalyst. This approach promises a sustainable polymerization route that ensures ease catalyst separation, reusability, and avoids the deoxygenation of the monomer mixture. *g*-CN was utilized together with radical mediator (triethylamine) as otherwise polymerization would proceed on the *g*-CN surface. Additionally, and for comparison purposes, commercial MeGVL was subjected to similar reaction conditions (which will be denoted as PMeGVL_R). After polymerization, precipitated and dried samples were investigated *via* ^{1}H-NMR and size exclusion chromatography (SEC). SEC results indicate polymer formation from the synthesized MeGVL (which will be denoted as PMeGVL_S) with a number of average molecular weight (M_n) of 4200 g mol^{-1} (~35 joined monomer units) and 6800 g mol^{-1} (~60 joined monomer units) for PMeGVL_R (**Figure S8**). In addition, molecular dispersities (*Đ*) of each polymer were found to be 1.92, which is a typical value for free radical polymerization mechanism. Furthermore, ^{1}H-NMR spectra of PMeGVL_S proved the suppression of vinylic hydrogen peaks (5.72 ppm and 6.03 ppm) which indicate the successful polymerization reaction and solvent removal **(Figure S9)**. The significant difference upon comparison of PMeGVL_R and PMeGVL_S is the appearance of the polymer, where PMeGVL_R is glass-like polymer with respect PMeGVL_S that found to be brown and non-glass-like polymer **(Figure 7)**. This observation is attributed to the presence of the side products in the withdrawn MeGVL synthesized sample. These results present the high

potential of utilizing biomass-derived compounds such as MeGVL as bio-based building blocks through a green polymerization process *via* visible light.

Conclusions

In this study, we have developed a sustainable process for the α-methylene-γ-valerolactone synthesis from γ-valerolactone using trioxane as a formaldehyde source in a continuous-flow system over a tailored Cs-loaded hierarchical beta catalyst. After an initial screening of commercial aluminosilicates with different topologies and Si/Al ratios, we identified beta zeolite with Si/Al ratio of 150 as a potential catalyst for this reaction. Based on previous studies that identified the occurrence of basic sites as beneficial for the selectivity towards the desired product, incorporation of Cs led to a substantial increase of the activity compared to the bulk material. The performance was further improved by the subsequent alkaline treatment to produce a hierarchical zeolite followed by the optimization of the Cs loading. The best-performing catalyst exhibited enhanced selectivity to α-methylene-γ-valerolactone with a productivity of 0.325 mmol min^{-1} g_{cat}^{-1}. This is attributed to the enhanced accessibility achieved by the introduction of mesoporosity along with the presence of basic sites of mild strength. Evaluation of this material in consecutive reaction-regeneration tests revealed that the catalyst performance slightly decreased in the second cycle, but the activity is retained during the third run, which was associated to the decrease of the basicity. The catalyst structure was preserved and the metal phase proved stable against leaching. As a proof of concept, the synthesized α-methylene-γ-valerolactone was subjected to visible-light-induced polymerization, reaching a final material with similar properties to poly(methyl) methacrylate. These findings pave the path for a large scale production of α-methylene-γ-valerolactone from cellulosic biomass, which can be readily polymerized towards a new and green generation of polymers.

Experimental Section

Materials

γ-Valerolactone (≥99%), 4-pentenoic acid (≥98%), cyanuric acid (98%), isopropanol (anhydrous, 99.9%), melamine (99%), methyl 4-pentenoate (≥95%), 2-butanol (>99.5%), 2-pentene (99%), pentanal (>97%), tetrahydrofuran (THF, GC grade), dioctyl ether (99%), sodium hydroxide (97%), cesium chloride (≥99%), triethylamine (98%), ammonium nitrate (≥98%), silica gel (SiO_2, grade 62), and and CsCl (99.9%) were purchased from Sigma-Aldrich. Cetyltrimethylammonium bromide (CTABr, 99%) was provided by Acros Organics. Lithium bromide (LiBr, anhydrous 99%) was purchased from Alfa Aesar. α-methylene-γ-valerolactone (stabilized with HQ, >97%) was obtained from TCI Chemicals. 2-methyltetrahydrofuran (MeTHF) (99%) was supplied from Carl Roth GmbH & Co. BETA zeolites (Si/Al = 150, 220) were provided by Clariant (HCZB 150) and TOSOH (980HOA), respectively. ZSM-5 (Si/Al = 140, CBV28014) and mordenite (Si/Al = 10, CBV21A) zeolites were provided by Zeolyst International. Zeolite X (Si/Al = 1.4) was purchased from Sigma Aldrich. All chemicals were used as received without further purification.

Catalyst preparation

Commercial Beta zeolites (beta-150, beta-220), where 150 and 220 refer to the nominal Si/Al ratio according to the manufacturer's specifications, were treated in an aqueous alkaline solution (0.2 M NaOH and 0.01 M CTABr) at 338 K for 30 min (30 cm^3 $g_{zeolite}^{-1}$) using an Easymax™ 102 reactor system (Mettler Toledo). The resulting slurry was quenched in ice-water, filtered, and the isolated solids washed extensively with deionized water and dried at 338 K. The resulting materials were converted into the H-form by three consecutive ion exchanges in aqueous ammonium nitrate solution (0.1 M, 338 K, 8 h, 100 cm^3 $g_{zeolite}^{-1}$) followed by calcination in static air at 823 K for 5 h using a heating rate of 5 K min^{-1}. Along the manuscript, the code H denotes the hierarchical materials. For the preparation of graphitic carbon nitride (*g*-CN) 1 g of cyanuric acid and 1 g melamine were mixed with 40 cm^3 of deionized water and stirred overnight. After centrifugation at 6000 rpm for 10 min, a precipitate was dried at 333 K under vacuum overnight and afterwards transferred into a capped crucible and calcined under N_2 atmosphere at 823 K for 4 h using a heating rate of 2.3 K min^{-1}.
Cs catalysts supported on Beta, H-Beta, ZSM-5, and mordenite zeolites, and SiO_2 were prepared *via* incipient wetness impregnation. The appropriate amount of CsCl was dissolved in deionized water targeting 5, 10, and 23 wt.% Cs loading followed by dropwise addition of the resulting solution into the zeolite support until slurry was formed. Subsequent drying was performed at 333 K in static air for 12 h. CsX was obtained by subjecting zeolite X to 3 subsequent ion-exchange treatments in aqueous solutions of CsCl (0.1 M, 8 h, 298 K, 100 cm^3 $g_{zeolite}^{-1}$). The catalysts in powder form were using hydraulics press (CARVER 3851CE) with 10 metric ton, crushed and sieved in the range of 250-500 μm to ensure a homogeneous flow of the reactant through the catalyst bed during the reaction. Prior the reaction, the catalyst was dried in static air at 393 K for 1 h (5 K min^{-1}) and calcined at 773 K for 5 h (5 K min^{-1}).

Catalyst Characterization

The metal content was determined by ICP-OES using an Optima 8000 ICP-OES from Perkin Elmer. Prior the analysis, the samples (0.01 g) were dissolved in a solution consisting of HCl (333 μL) and HNO_3 (167 μL). Powder XRD measurements were performed on a Bruker D8 diffractometer. The X-rays source was Cu-Kα (λ = 0.154 nm) equipped with a scintillation counter-Scinti-Detector. The diffraction data was recorded in the 4-70° 2θ range with an angular step of 0.05° and a continuing time of 2 s per step. Ar sorption at 77 K was undertaken in Micromeritics TriStar II instrument. Prior to the measurement, the samples were evacuated at 573 K for 3 h. Temperature-programmed desorption of carbon dioxide (CO_2-TPD) was performed in a Micromeritics Autochem II 2920 analyzer. First, the solid (0.1 g) was loaded into a U-shaped quartz micro-reactor, pretreated in He (20 cm^3 min^{-1}) at 423 K for 2 h, and cooled to 323 K. Thereafter, CO_2 was chemisorbed at 323 K in 50 consecutive pulses with a 5 vol.% CO_2/He mixture (1 cm^3 STP per pulse) followed by purging with He (10 cm^3 STP min^{-1}) at the same temperature for 90 min. Desorption of CO_2 was monitored in the range of 323-973 K using a heating rate of 10 K min^{-1} and a He flow of 20 cm^3 STP min^{-1}.The scanning transmission electron microscopy (STEM) study of selected samples was performed using a double Cs corrected JEOL JEM-ARM200F (S)TEM operated at 80 kV and equipped with a cold-field emission gun, with a high-angle silicon drift Energy Dispersive X-ray (EDX) detector (solid angle up to 0.98 steradians with a detection area of 100 mm^2), and a Gatan Imaging Filter (GIF Quantum). For STEM observation, samples were put onto a lacey carbon film supported on a Cu grid. Annular dark field scanning transmission electron microscopy (ADF - STEM) images were collected at a probe convergence semi-angle of 25 mrad. XPS measurements were carried out under ultra-high vacuum (UHV) 1.5×10^{-8} Pa (CISSY equipment) equipped with SPECS XR 50 X-

ray gun with Al Kα radiation (1486.6 eV) and combined with lens analyzer module (CLAM). The binding energy scale was calibrated using Au $4f_{7/2}$ (84.0 eV) band as reference. The binding energy and quantitative analysis were performed utilizing "peakfit" and "Igor" software and using Lorenzian-Gaussian functions and Shirley background deletion in photoemission spectra. Thermogravimetric analysis (TGA) was performed *via* TG 209 Libra from Netzsch. Typically, 50 mg of used catalyst sample was dried at 423 K for 2 h. Then, the sample was heated to 1273 K with a heating rate of 10 K min^{-1}. Fourier transform infrared spectroscopy (FTIR) of adsorbed pyridine was conducted in a Bruker IFS 66 spectrometer (650-4000 cm^{-1}, 4.0 cm^{-1} optical resolution, co-addition of 32 scans). Self-supporting wafers of catalyst (5 ton m^{-2}, 0.03 mg, 1 cm^2) were degassed under vacuum (10^3 mbar) for 4 h at 693 K, prior to adsorbing pyridine at room temperature. Gaseous and weakly adsorbed molecules were subsequently removed by evacuation at 673 K for 30 min. The total concentrations of Brønsted and Lewis acid sites were calculated from the band area of adsorbed pyridine at 1545 and 1454 cm^{-1}, using a previously determined extinction coefficient of $\varepsilon_{Brønsted}$ = 1.67 cm $mmol^{-1}$ and ε_{Lewis} = 2.94 cm $mmol^{-1}$.

Catalytic evaluation

The γ-valerolactone (GVL) upgrading to α-methylene-γ-valerolactone (MeGVL) in the presence of trioxane as a formaldehyde (FA) source was studied in a homemade continuous-flow fixed-bed reactor (**Figure S1A**) comprising (i) an HPLC pump equipped with a pressure sensor (Jasco PU-2080 plus), (ii) a two-sides opened oven equipped with a heat controller (Model # 4848 from Parr Instrument Company), and (iii) a sampling unit equipped with a back pressure regulator and a cooling trap. To ensure an efficient heat transfer from the oven to the fixed-bed reactor, an aluminum cylinder with 3 different holes was placed inside the oven (**Figure S1B**), *i.e.*, a 1/16" hole as pre-heating unit to heat the reactant to the desired reaction temperature before its get in contact with catalyst bed, a 1/4" hole to place the fixed-bed reactor (HPLC blank column from Supelco was used as tubular reactor - inner diameter = 4.6 mm, outer diameter = 1/4" and length = 25 cm) and a third hole for the thermocouple (Model # A472E5 from Parr Instrument Company).
In a typical experiment, the reaction solution (5.1 g of GVL and 10.1 g of trioxane which equal to molar ratio of 2) in 500 cm^3 of MeTHF) was fed *via* the HPLC pump at a rate of 0.3 cm^3 min^{-1} through the pre-heating unit prior to the catalytic reactor ($m_{catalyst}$ = 3 g for bulk materials and 2 g for the hierarchical counterparts). The reactor temperature and pressure were kept at ambient for 15 min, after which the temperature was increased to the target value, *i.e.*, 553 K, 568 K or 583 K, and the system pressurized to 6 MPa, allowing an average residence time (τ) of 13.8 min. Samples (2 cm^3) were collected once the steady state was reached (after *ca.* 45 min). To 1 cm^3 of the samples, 50 μL of dioctyl ether as internal standard was added. After the reaction, the catalyst was washed with acetone (45 cm^3) and dried at 333 K for 12 h in static air. Regeneration of the catalyst was conducted *via* thermal treatment in static air at 823 K for 5 h (5 K min^{-1}). Product analysis was conducted using an off-line gas chromatograph equipped with a HP-5MS column (inner diameter = 0.25 mm, length = 30 m and film = 0.25 μm) coupled to a mass spectrometer (Agilent GC 6890, Agilent MSD 5975) and a gas chromatograph (Agilent GC 6890) equipped with a FID detector and a HP-5 column (inner diameter = 0.25 mm, length = 30 m and film = 0.25 μm). The temperature program starts at 323 K (hold time = 2 min) and raises up to 573 K (30 K min^{-1}, hold time = 2 min). The rates of GVL conversion (r_{GVL}) and formation of the reaction products *i* (r_i) were calculated according to the following equations:

$$r_{GVL}\left(\mathrm{mmol_{GVL}\,min^{-1}\,g_{cat}^{-1}}\right)=\frac{c_{GVL}}{\left(m_{cat}/N_{GVL}^{0}\right)} \qquad \text{Eq. (1)}$$

$$r_{i}\left(\mathrm{mmol_{i}\,min^{-1}\,g_{cat}^{-1}}\right)=\frac{c_{i}}{\left(m_{cat}/N_{GVL}^{0}\right)} \qquad \text{Eq. (2)}$$

where $c_{GVL\ or\ i}$ refer to the concentration of GVL and products in mmol cm^{-3}, respectively in the withdrawn sample, m_{cat} is catalyst mass in g and N_{GVL}^{0} is the initial molar flow of GVL in cm^3 min^{-1}.

Visible-light-induced MeGVL polymerization

Commercial MeGVL and the synthesized MeGVL from GVL using 5Cs/H-beta-150 at 568 K were subjected to polymerization reactions using *g*-CN. In the first case, 1.0 cm^3 of commercial MeGVL was mixed with 10 mg of *g*-CN and 0.05 cm^3 of trimethylamine. The resulting mixture was subsequently illuminated with visible light for 3 h at room temperature after which an increase in viscosity was observed. *g*-CN was removed by centrifugation and the remaining solution poured into methanol to precipitate the poly(MeGVL) which will be considered as a reference polymer (PMeGVL_R). The white precipitate was filtered and dried overnight at 333 K. Polymerization of the synthesized MeGVL was conducted after evaporation of the MeTHF. A 1 cm^3 of MeGVL was mixed with 10 mg of *g*-CN, 1 cm^3 of isopropyl alcohol and 0.05 cm^3 of trimethylamine followed by illumination with visible light for 16 h at room temperature. Similarly, to the case where the commercial MeGVL was used, an increase in viscosity was detected. After centrifugation, the mixture was added into deionized water to precipitate the poly MeGVL_Sample which is denoted (PMeGVL_S). The resulting precipitate was filtered and dried overnight at 333 K. It is important to note that increasing drying temperature influences darkening of the polymer product and that commercial MeGVL polymerization with similar conditions show considerably low yield. Size exclusion chromatography (SEC) of the PMeGVL_R and PMeGVL_S was conducted in THF with 0.05 M of LiBr and BSME as internal standard using a PSS GRAM 100/1000 column (8×300 mm, 7 μm particle size) with a PSS GRAM pre-column (8×50 mm), a Shodex RI-71 detector and a calibration with PMMA standards from PSS. PMeGVL_S were analyzed by ^{1}H NMR using a Bruker Avance 400 spectrometer. Prior to the analysis, 1 cm^3 of dimethyl sulfoxide-d6 (DMSO) was added to 200 μl of PMeGVL_S.

Acknowledgements

The authors are grateful for the financial support from Max-Planck Society. Scientific discussions, suggestions, feedback and support from Prof. Dr. Markus Antonietti is gratefully acknowledged. Also, thanks to the Electrical and Mechanical Workshops at Max Planck Institute of Colloids and Interfaces for their technical contributions to our research project. Thanks are also due to Irina Shekova, Jessica Brandt, Katharina Otte, Marlies Gräwert and Antje Völkel from Max Planck Institute of Colloids and Interfaces for XRD, ICP-OES, SEC and TGA measurements, respectively. Dr. Iver Lauermann from Helmholtz Zentrum Berlin PVComB is acknowledged for XPS measurements. Dr. Silke Sauerbeck from Clariant is greatly acknowledged for supplying the zeolite sample. The authors are thankful to Alaa Al-Naji for the idea and design of the graphical abstract.

Keywords: basic catalysis • flow chemistry • lignocellulosic biomass • α-methylene-γ-valerolactone • γ-valerolactone

[1] D. Esposito, M. Antonietti, *Chem. Soc. Rev.* **2015**, *44*, 5821-5835.
[2] N. Brun, P. Hesemann, D. Esposito, *Chem. Sci.* **2017**, *8*, 4724-4738.
[3] P. C. Bruijnincx, B. M. Weckhuysen, *Angew. Chem.* **2013**, *125*, 12198-12206; *Angew. Chem. Int. Ed.* **2013,** *52,* 11980-11987.
[4] A. Corma, S. Iborra, A. Velty, *Chem. Rev.* **2007**, *107,* 2411-2502.

[5] A. J. Ragauskas, C. K. Williams, B. H. Davison, G. Britovsek, J. Cairney, C. A. Eckert, W. J. Frederick, J. P. Hallett, D. J. Leak, C. L. Liotta, J. R. Mielenz, R. Murphy, R. Templer, T. Tschaplinski, *Science* **2006**, *311,* 484-489.

[6] E. L. Kunkes, D. A. Simonetti, R. M. West, J. C. Serrano-Ruiz, C. A. Gärtner, J. A. Dumesic, *Science* **2008**, *322,* 417-421.

[7] B. O. De Beeck, M. Dusselier, J. Geboers, J. Holsbeek, E. Morré, S. Oswald, L. Giebeler, B. F. Sels, *Energy Environ. Sci.* **2015**, *8,* 230-240.

[8] http://www.nrel.gov/docs/fy04osti/35523.pdf_accessed on 18.12.2018.

[9] J. A. Dumesic, D. A. Simonetti, E. L. Kunkes, US Patent No. 0116449 A1, **2013**.

[10] B. Girisuta, L. P. B. M. Janssen, H. J. Heeres, *Ind. Eng. Chem. Res.* **2007**, *46,* 1696-1708.

[11] J. Q. Bond, D. M. Alonso, D. Wang, R. M. West, J. A. Dumesic, *Science* **2010**, *327,* 1110-1114.

[12] D. Albani, Q. Li, G. Vilé, S. Mitchell, N. Almora-Barrios, P. T. Witte, N. López, J. Pérez-Ramírez, *Green Chem.* **2017**, *19,* 2361-2370.

[13] T. Ennaert, J. Van Aelst, J. Dijkmans, R. De Clercq, W. Schutyser, M. Dusselier, D. Verboekend, B. F. Sels, *Chem. Soc. Rev.* **2016**, *45,* 584-611.

[14] I. T. Horváth, H. Mehdi, V. Fábos, L. Boda, L. T. Mika, *Green Chem.* **2008**, *10,* 238-242.

[15] M. Al-Naji, A. Yepez, A. M. Balu, A. A. Romero, Z. Chen, N. Wilde, H. Li, K. Shih, R. Gläser, R. Luque, *J. Mol. Catal. A: Chem.* **2016**, *417,* 145-152.

[16] C. Wei, D. Esposito, K. Tauer, *Polym. Degrad. Stab.* **2016**, *131,* 157-168.

[17] W. J. McGraw, US Patent No. 2624723, **1953**.

[18] A. Tanaka, K. Yamashita, *Agric. Biol. Chem.* **2014**, *42,* 1585-1588.

[19] Z. Vobecka, C. Wei, K. Tauer, D. Esposito, *Polymer* **2015**, *74,* 262-271.

[20] L. E. Manzer, K. W. Hutchenson, US Patent No. 6649776 B2, **2003**.

[21] L. E. Manzer, *Appl. Catal., A* **2004**, *272,* 249-256.

[22] K. Doi, E. Togano, S. S. Xantheas, R. Nakanishi, T. Nagata, T. Ebata, Y. Inokuchi, *Angew. Chem.* 2013, *125*, 4476-4479; *Angew. Chem. Int. Ed.* **2013**, *52*, 4380-4383.

[23] G. Wang, C. Sararuk, Z. X. Li, C. S. Li, *AIChE J.* **2018**, *4*, 1359-1372.

[24] A. W Schnizer, G. J Fisher, US Patent No. US2714616A, **1955**.

[25] M. Shalom, S. Inal, C. Fettkenhauer, D. Neher, M. Antonietti, *J. Am. Chem. Soc.* **2013**, *135*, 7118-7121.

[26] B. Kiskan, J. Zhang, X. Wang, M. Antonietti, Y. Yagc, *ACS Macro Lett.* **2012**, *1*, 546-549.

[27] B. Kumru, V. Molinari, M. Shalom, M. Antonietti, B. V. K. J. Schmidt, *Soft Matter.* **2018**, *14*, 2655-2664.

[28] B. Kumru, V. Molinari, R. Dünnebacke, K. G. Blank, B. V. K. J. Schmidt, *Macromol. Rapid Commun.* **2018**, DOI: 10.1002/marc.201800712.

[29] G. M. Lari, B. Puértolas, M. S. Frei, C. Mondelli, J. Pérez-Ramírez, *ChemCatChem* **2016**, *8*, 1507-1514.

[30] T. C. Keller, M. Položij, B. Puértolas, H. V. Thang, P. Nachtigall, J. Pérez-Ramírez, *J. Phys. Chem. C* **2016,** *120*, 4954-4960.

[31] Y. Ono, H. Hattori in *Solid Base Catalysis*, Springer, **2012**, pp. 180.

[32] A. A. Lemonidou, L. López, L. E. Manzer, M. A. Barteau, *Appl. Catal., A* **2004**, *272,* 241-248.